Microfluid Nanofluid (2012) 13:579–588
DOI 10.1007/s10404-012-0974-y

RESEARCH PAPER

Dynamics of a microchain of superparamagnetic beads in an oscillating field

Yan-Hom Li · Ching-Yao Chen · Shih-Tsung Sheu · Jay-Min Pai

Received: 3 January 2012 / Accepted: 27 March 2012 / Published online: 25 April 2012

Abstract The dynamics of microchains containing superparamagnetic particles in an oscillating field are studied experimentally. The chains are first formed by a static directional field, and then manipulated by an additional dynamical perpendicular field. The present methodology represents a simple reversible chaining process, whose particles can be re-dispersed after removal of the field. The motion of superparamagnetic chains is dominated by magnetic torque and induced hydrodynamic drag. The effects of key parameters, such as field strengths and the lengths of particle chains, are thoroughly analyzed. Distinct behaviors, from rigid body oscillations and bending distortions to rupture failures, are observed by increasing the amplitudes of oscillating fields or chains' lengths. Because of lower induced drag, a shorter chain follows the field trajectory closely and oscillates more synchronically with the external field. On the other hand, the influences of field strengths are not consistent. Even the overall oscillating phase trajectory in a stronger external field deviates less significantly from the corresponding field trajectory, a stronger dynamical component of the external field results in larger phase angle lags at certain points. The experimental results confirm the criterion of ruptures can be effectively determined by the value of ($N^*Mn^{1/2}$), where Mn is the Mason number defined as the ratio of induced drag to dipolar attraction, and N represents the number of particles contained in a chain.

Keywords Oscillating field · Micro-superparamagnetic chain · Magnetic particle · Mason number

Y.-H. Li · C.-Y. Chen (✉) · S.-T. Sheu · J.-M. Pai
Department of Mechanical Engineering, National Chiao Tung University, Taiwan, Republic of China
e-mail: chingyao@mail.nctu.edu.tw

1 Introduction

Magnetorheological (MR) suspension is an artificial and smart fluid consisting of paramagnetic solid particles suspended in a non-magnetic solvent. Due to the paramagnetism of these particles, they are applicable to reversible microdevices in biotechnical applications and micro-electromechanical systems (MEMS), such as micromixers (Biswal and Gast 2004a; Kang et al. 2007; Roy et al. 2009; Martin et al. 2009), microswimmers (Dreyfus et al. 2005; Li et al. 2012), and other microfluidics (Terray et al. 2002; Gijs 2004). The most common way of enhancing micromixing is chaining and manipulating the particles in a rotational field (Biswal and Gast 2004a; Kang et al. 2007; Roy et al. 2009), while Martin et al. (2009) controlled the magnetic chain in a so-called vortex magnetic field.

Because of the great popularity of micromixing device in a rotational field, particle chains under a rotating magnetic field have been an extensively studied subject in recent years. The dynamics and aggregation processes of magnetorheological fluids subject to rotating magnetic fields have been investigated experimentally (Melle et al. 2000, 2002a, b; Vuppu et al. 2003) and numerically (Kang et al. 2007; Petousis et al. 2007). It has been concluded the governing parameters of such a rotating chain are the Mason number (Melle and Martin 2003; Melle et al. 2003), which determines the ratio between magnetic attraction and hydrodynamic drag, as well as the chain's length (or the number of particles contained in the chain). When these parameters exceed certain critical values, rupture occurs within the early transient time period, mainly near the chain's center (Melle and Martin 2003; Petousis et al. 2007). Nevertheless, the positions of the fracture might relocate due to variations in bead susceptibility. In addition, both brittle or ductile chain fracture are observed, depending on the permeability of the

particles (Melle and Martin 2003). The critical length to prevent rupture is proposed to be inversely proportional to the square root of the Mason number (Melle and Martin 2003). Besides, Biswal and Gast (2004a, b) also investigated the motion of magnetic particles permanently linked by flexible chemistries in a rotating field.

Microchains subjected to an oscillating field have drawn much less attention compared to in a rotational field. It should be noticed that the experimental setup for such an oscillating field is similar to a rotating field, and the implementation to a MEMS or Lab-on-a-Chip is straightforward (Petousis et al. 2007; Lacharme et al. 2009; Weddemann et al. 2011; Karle et al. 2011; Wittbracht et al. 2012). An oscillating microchain consisting of magnetic particles has been successfully applied to mimic a microswimmer (Dreyfus et al. 2005; Li et al. 2012). Dreyfus et al. (2005) connected microsize magnetic particles by nano-size DNA to provide stronger inter-particle bonding forces. The chain was then attached to a larger biological cell, for example, a red blood cell, and manipulated in an oscillating field to move forward. Li et al. (2012) chained superparamagnetic particles of different sizes to mimic an artificial swimmer. Sufficient propulsion was generated to drive the chain in a swimming motion. Nevertheless, the efficiencies of their artificial swimming devices are much lower than natural swimmers. To effectively employ an oscillating microchain as a microswimmer or to other MEMS applications, detailed understandings of the dynamics and behaviors are essential. The tasks of realizing such an oscillating chain are more challenging than its rotational counterpart due to the strong transient phenomena, for instance, significant variation of angular speed within a period of oscillation. In this paper, the emphasis lies on the synchronicity of the phase angle trajectory between the oscillating magnetic particle chain and the external field. The influences of the control parameters, such as field configuration and length of the chain, are analyzed systematically. In addition, the criteria that might lead to structure fracture is also examined.

2 Experimental setup

The experimental configuration is schematically demonstrated in Fig. 1. Microsize magnetic particles are initially dispersed in distilled water. The magnetic particles used in our experiments are aqueous superparamagnetic polystyrene microspheres coated with iron oxide grains produced by Invitrogen Life Tech. The mean radius of the microspheres (denoted as a) are $a = 2.25$ μm, with a susceptibility of $\chi = 1.6$ and no magnetic hysteresis or remanence. The field strength, at which magnetization of beads starts to appear saturated is between 350 and 400 Oe. A static unidirectional magnetic field, denoted as H_d, is generated first by a pair of coils powered by DC power sources. Magnetic particles magnetized by the unidirectional field tend to aggregate and form chains because of dipolar attractive forces. To create an oscillating field, another pair of coils are placed perpendicularly to the former pair and connected to AC power supplies to generate a sinusoidal dynamical perpendicular field (H_v) with a maximum field strength H_p and frequency f, i.e., $H_v = H_p \sin(2\pi ft)$. This additional perpendicular field and the original static directional field result in an overall oscillating field ($\vec{H}$) of $H = H_d i + H_v j$, in which $\vec{i}$ and $\vec{j}$ are unit vectors in the directional and perpendicular axis, respectively. Under such a field configuration, the phase angle trajectory (θ) of the external field is prescribed as $\theta(t) = \tan^{-1}[(H_p/H_d)\sin(2\pi ft)]$ associated with an amplitude (denoted as θ_{Amax}) of $\theta_{\mathrm{Amax}} = \tan^{-1}(H_p/H_d)$. The magnetic particle chains, which tend to align along the orientation of the external field, would oscillate under the presence of such an oscillating field. The motion of the particle chains is recorded by an optical microscope connected to a digital camera (Silicon Video 643C) whose shooting rate is 200 frames/s. The snapshot images are transferred to an image software (Ulead GIF Animator) for further analysis. Representative snapshot images, which are modified from the recorded movies (http://www.youtube.com/user/athomeli#p/u) by improving their contrasts and resolutions, are presented in the following sections to identify the distinct behaviors of particle chains under various conditions.

3 Results and discussion

3.1 An oscillating chain

Figure 2 shows the sequential images taken from a chain consisting of nine particles (denoted as P9) subjected to an oscillating field configuration of $H_d = 24.15$ Oe (noted 1 Oe = 1,000/4π A/m), $H_p = 29.02$ Oe and $f = 1$ Hz (or period $P = 1$ s) within one and half periods, i.e., $0 \leqq t \leqq 3P/2$. We like to point out, a rotating frequency applied in a micromixer could be as low as 5 rpm in early literatures (Roy et al. 2009). Nevertheless, a much higher frequency of O(10) Hz is usually needed to practically drive a microswimmer (Dreyfus et al. 2005; Li et al. 2012). In the present study, an intermediate frequency is experimented to ensure the images are properly analyzed. The corresponding amplitude of the external field is obtained as $\theta_{\mathrm{Amax}} = 50°$. Under such a condition, the chain behaves as a rigid beam and oscillates along the orientation of the external field, for example, counter-clockwise at $t < P/4$ and $3P/4 < t < 5P/4$, clockwise at $P/4 < t < 3P/4$ and $5P/4 < t < 3P/2$. The instantaneous phase angle lag (denoted

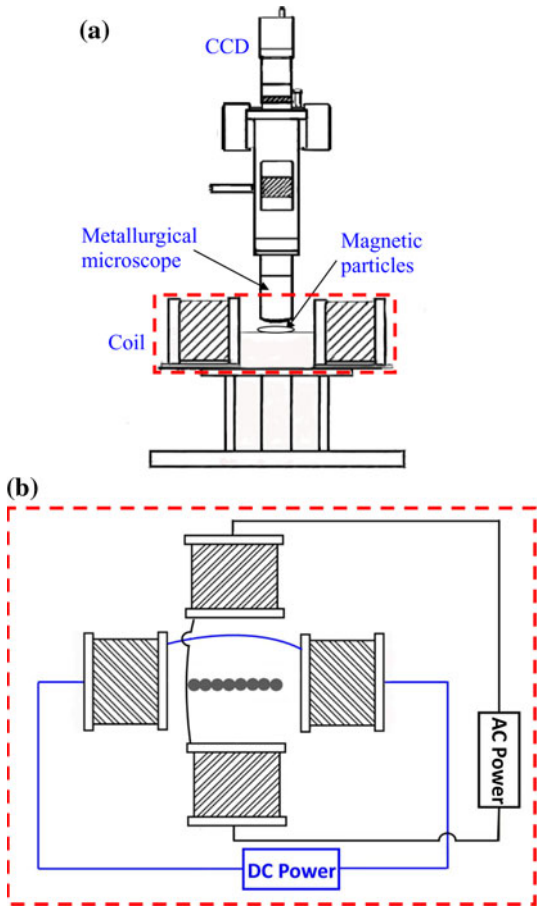

Fig. 1 **a** Schematic of experimental setup, and **b** *top view* configuration of coil pairs for generation of oscillating magnetic field. The size of the particle chain in (**b**) is exaggerated and not in actual scale

as $\Delta\theta_L$ in images) is not that significant in the present situation. A complete evolution of phase angle trajectory can be constructed accordingly, which is shown in Fig. 3a. It is noticed an increasing positive value of the phase angle stands for a counter-clockwise motion, and vice versa. After an initial transient stage caused by the sudden start, both the frequency and amplitude of the chain's oscillating trajectory reveal close similarities associated with a slight shift toward the later time (i.e., time delay) compared to the trajectory of the external field. Note, the slightly larger amplitude of the chain ($\theta_{Amax} = 51.5°$ at the second peak) than the external field is due to inertial effects.

In practical manipulations of a microchain, it is important to analyze the actual motion of the chain compared to the input external field. As demonstrated in Figs. 2 and 3, several measurements are helpful to provide the desired information, such as the time delay of the chain's oscillating phase trajectory as well as its actual amplitude and instantaneous phase angle lags. In the following discussion, the influences of major parameters on these measurements are evaluated.

3.1.1 Influences of chain's length

It is well known the motion of a magnetic chain is dominated by the competition between magnetic forces and induced hydrodynamic drags. When a chain composed of N particles is under a rotational field, the chain experiences a magnetic torque (M^m) and an opposing viscous drag (M^v) given as (Melle et al. 2003a; Biswal and Gast 2004b; Roy et al. 2009)

$$M^m = \frac{\mu_0\mu_s}{4\pi}\frac{3|\vec{m}|^2N^2}{2(2a)^3}\sin(2\Delta\theta_L), \quad (1)$$

$$M^v = \frac{4}{3}N\pi a^3\frac{2N^2}{\ln(N/2)}\eta\omega. \quad (2)$$

Here μ_0 and μ_s stand for the vacuum permeability and the relative permeability of the solvent, respectively. $\vec{m}$ is the dipole moment of a magnetic particle, and η is the solvent fluid viscosity. The angular speed of the chain is represented by ω. The almost synchronous rigid body oscillation of the P9 chain, shown in Figs. 2 and 3, is a consequence of relatively weaker induced drag, compared to magnetic torque, at that particular condition. If the chain's length is increased to contain 21 particles (P21) subjected to an identical field configuration, more severe phase angle lags associated with apparent bending deformation to an S shape are observed, as shown in Fig. 4. It is expected a longer chain length (a greater number of N) leads to a stronger drag locally, as indicated in Eq. (2). The stronger drag reduces instantaneous angular speeds, and results in more significant phase lags. In addition, the moment arms to outer particles are increased as well. The stronger drag associated with longer moment arms generate excessive bending moment locally, and distort the shape of the particle chain. Nevertheless, the radial dipolar attractions are still sufficiently strong to sustain a chaining formation. A similar stable S shape deformation is also reported in a rotational field (Melle et al. 2003; Petousis et al. 2007; Li et al. 2012).

The influences of chain's lengths can be further analyzed by complete evolutions of the phase angle trajectories shown in Fig. 3. The amplitude of the present P21 chain ($\theta_{Amax} = 36°$) is much smaller than the external field, even an identical frequency of $f = 1$ Hz is still well preserved. In addition, the shift toward the later time (time delay) of the phase trajectory is more apparent. While the peaks (including the lower and higher peaks) of externally filed trajectories appear at ideal times of $t = P/4$, $3P/4$ and $5P/4$, the peaks of the P9 chain are observed slightly later at $t = 3P/10$, $8P/10$ and $13P/10$. As to the longer P21 chain, these peaks are further delayed to $t = 4P/10$, $14P/15$ and $43P/30$. The smaller

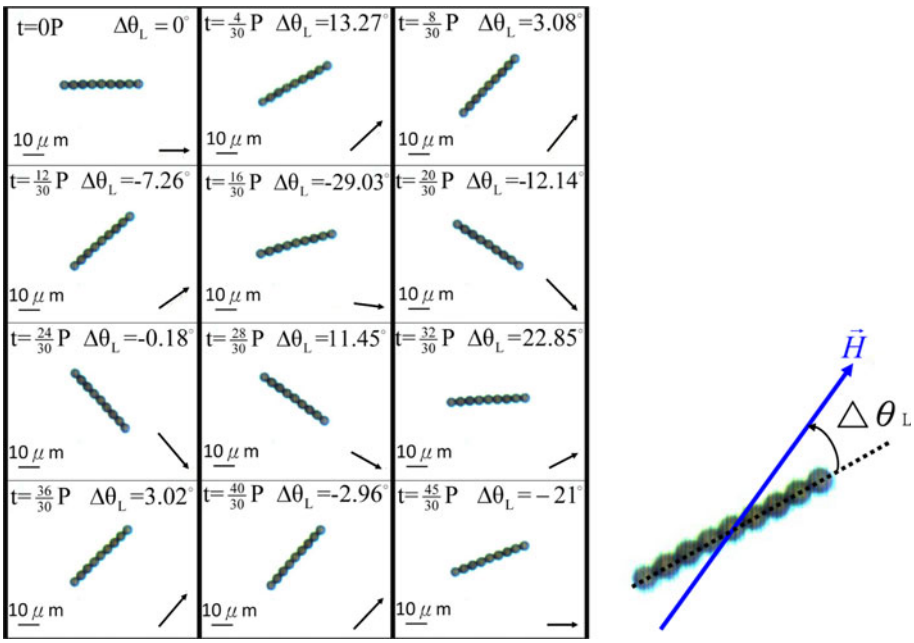

Fig. 2 Images of 9-particle (P9) chain oscillating under the field configuration of $H_d = 24.15$ Oe, $H_p = 29.02$ Oe and $f = 1$ Hz. The *black arrows* inside images represent the strength and orientation of the overall field. The magnetic chain oscillates along the external field but lags behind by insignificant phase angles (denoted as $\Delta\theta_L$). The phase lag ($\Delta\theta_L$) is measured by the angle between the centerline of the chain and the orientation of the overall field

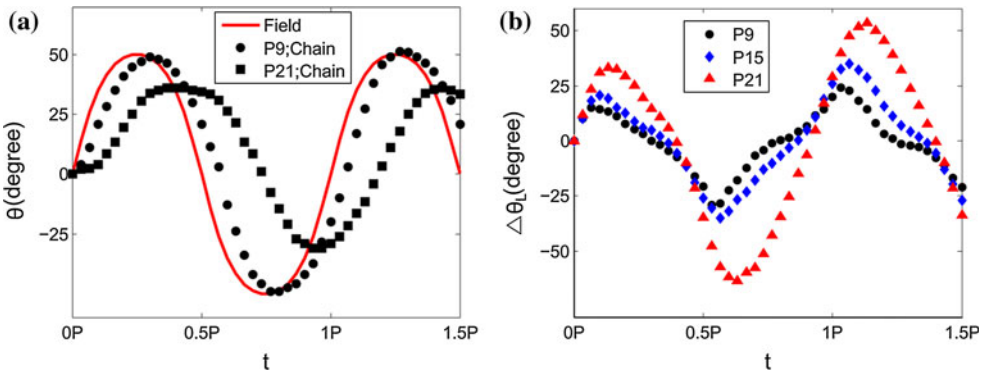

Fig. 3 **a** Trajectories of the phase angle (θ) of the external field of P9 chain (images shown in Fig. 2) and P21 chain (images shown in Fig. 4). The amplitudes of longer chains are smaller associated with longer time delays. **b** Evolutions of phase angle lag ($\Delta\theta_L$) of chains composed of different numbers of particles. Larger phase lags result from stronger induced drags by longer chains

oscillating amplitude associated with a more significant time delay of P21 chain indicates a stronger viscous dissipation.

The facts of a smaller amplitude associated with the same frequency confirms a slower angular speed in the present case of a longer length. The reduced angular speed causes chain lagging behind the external field by a more significant phase angle. When the field has reached its peak of $\theta_{Amax} = 50°$ at $t = P/4$, the P21 chain has just moved to a phase angle of $\theta = 30.5°$. Afterward, the orientation of the external field has reversed in the clockwise direction. Within the time at $P/4 < t < 2P/5$, since the field orientation is still ahead of the orientation of the P21 chain (or the phase angle of the external field is greater than the P21 chain, as shown in Fig. 3a), the chain continuously oscillates counter-clockwise. Nevertheless, the movement is very insignificant, and results in a flatter peak. After the crossover of the trajectories at $t = 2P/5$, the P21 chain would follow the external field and reverses its oscillation in the clockwise direction. Similar scenarios occur at the later peaks.

More detailed insights regarding the motion of particle chains can be further understood by the phase angle lags ($\Delta\theta_L$). According to the expression of Eq. (1), a counter-clockwise torque is generated by a positive $\Delta\theta_L$, and vice versa. Figure 3b shows the evolutions of the phase lags for chains consisting of various numbers of particles, for example, P9 chain, P15 chain and P21 chain. One observation is larger phase lags result from longer chains. In addition, the patterns again appear periodically after the initial stages affected by sudden movements. In addition, the maxima of the phase lags are shifted toward later times for longer chains, which is similar to their corresponding phase trajectories shown in Fig. 3a. It is noticed that detailed understandings of the correlation between of phase lags and the lengths of chains rely on the solutions of non-linear Navier–Stokes equations. Nevertheless, it can be

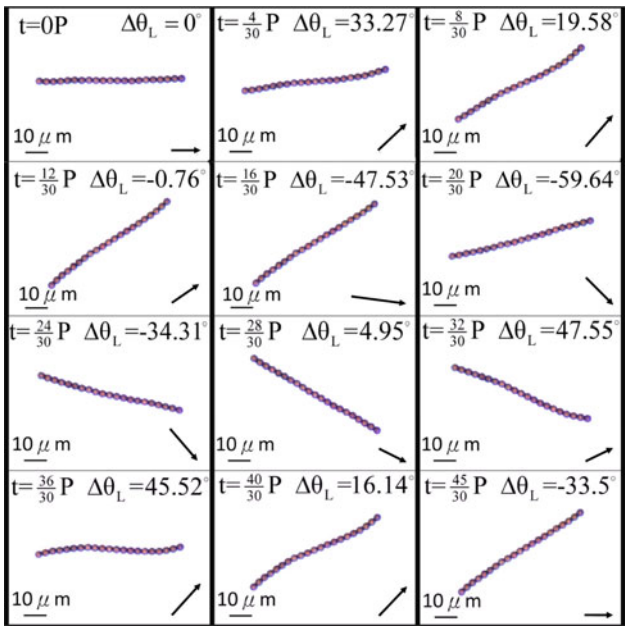

Fig. 4 Images of a 21-particle (P21) chain oscillating under a field configuration of $H_d = 24.15$ Oe, $H_p = 29.02$ Oe and $f = 1$ Hz. The particle chain undergoes apparent deformation associated with more significant instantaneous phase lags

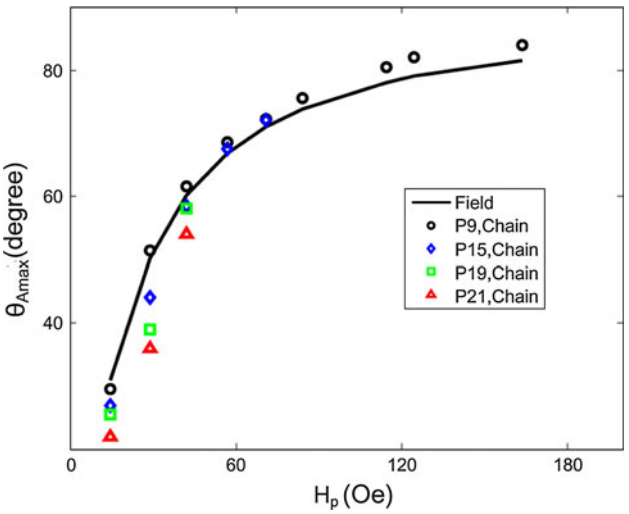

Fig. 5 Amplitudes (θ_{Amax}) of chains composed of different numbers of particles subjected to various perpendicular field strengths in a fixed directional field of $H_d = 24.15$ Oe and $f = 1$ Hz. The theoretical amplitudes of the external fields are indicated by a *solid line*. More severe energy dissipation of longer chains results in smaller amplitudes. The amplitudes of shorter chains might exceed the external field in stronger field strengths due to significant inertial effects

generally expected that a longer chain would induce stronger drags under the same field condition, and thus leads to a larger phase angle lag.

The effects of larger phase lags and shifts toward later times for chains of longer lengths have important implications for the oscillating features of chains. As indicated in Eq. (1), magnetic torque increases for a larger phase lag within the range of $\Delta\theta_{\mathrm{L}} < 90°$ but changes sign for a negative $\Delta\theta_{\mathrm{L}}$. As a result, the oscillating orientation reverses at the time of the vanishing phase lag, i.e., counter-clockwise or clockwise for $\Delta\theta_{\mathrm{L}} > 0$ and $\Delta\theta_{\mathrm{L}} < 0$, respectively. Consequently, the peaks of the phase trajectories would occur at the reversing timings of $\Delta\theta_{\mathrm{L}} = 0$, if the inertial effects are neglected. Figure 3b clearly shows the reversing times are later for longer chains, which confirm observations from the phase angle trajectories shown in Fig. 3a.

It is also practical to record the actual amplitudes of the particle chains (θ_{Amax}) shown in Fig. 5. This measurement can be compared with the theoretical amplitude of the external field, i.e., $\theta_{\mathrm{Amax}} = \tan^{-1}(H_p/H_d)$, and serves as an indicator regarding the effectiveness of the oscillating device. Under a fixed field condition, a longer chain always results in a smaller amplitude. This is in line with common expectation that more energy is dissipated by the stronger viscous effects of a longer chain. At the present field configuration, amplitudes are measured as $\theta_{\mathrm{Amax}} = 36°$, 39°, 44° and 51.5° for P21, P19, P15 and P9 chain, respectively.

3.1.2 *Effects of perpendicular field strength*

The effects of field strengths on the motion of microchains are first examined by raising the perpendicular field strength H_p while fixing the directional field at $H_d = 24.15$ Oe and frequency at $f = 1$ Hz. Figure 6 demonstrates the sequential motion of a P9 chain subjected to the representative strength of $H_p = 124.48$ Oe, which can be directly compared with the case shown in Fig. 2. The stronger perpendicular field leads to a larger amplitude of oscillation and more significant phase lags at certain instants. Nevertheless, the chain still oscillates rigidly.

More systematic comparisons can be made by Fig. 7a, which depicts the phase trajectories under three field strengths, for example, $H_p = 29.02, 70.88, 124.48$ Oe. Note, the chain in the strongest perpendicular field of $H_p = 124.48$ Oe oscillates almost synchronously with the external field without significant time delay. This interesting feature is attributed to a flatter trajectory pattern of the external field for a stronger perpendicular field, as shown in Fig. 7a. The flatter phase trajectory leads to faster angular speeds near $t = 0$, $P/2$, P and $3P/2$. As a result, significant phase lags occur near these times. Detailed information regarding the phase lags is demonstrated in Fig. 7b, indicating $|\Delta\theta_{\mathrm{L}}| = 69°$ at $t = 8P/15$, $31P/30$ and $23P/15$. The significant phase lags generate larger magnetic torque (Eq. 1) to drive the magnetic chain. On the other hand, very slow angular speeds are driven near the peaks, i.e., $t = P/4$, $3P/4$ and $5P/4$ in Fig. 7a, when the phase trajectory is nearly

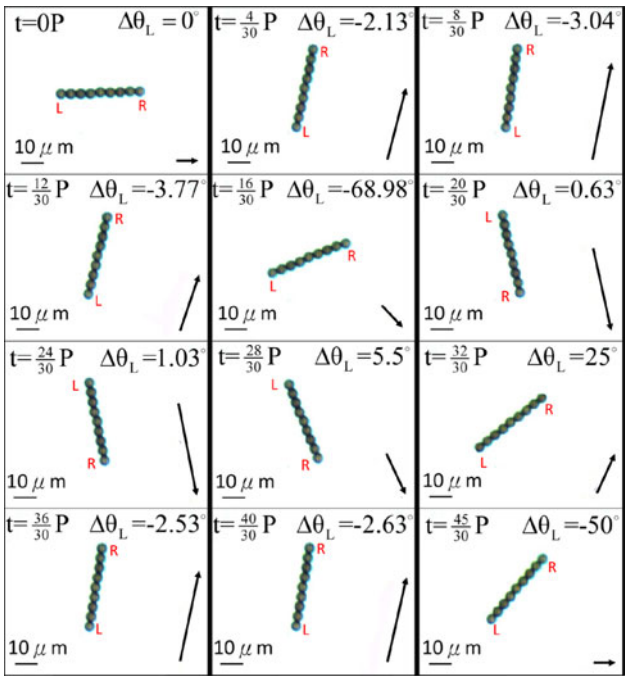

Fig. 6 Images of 9-particle (P9) chain oscillating in a stronger perpendicular component of $H_d = 24.15$ Oe, $H_p = 124.48$ Oe and $f = 1$ Hz. Chain oscillations are rigidly associated with larger phase lags at certain instants. Marks of *L* and *R* represent the left and right ends of the chain, respectively

flat, so both the motion of the field and chain are very insignificant and nearly stagnant. This almost stagnant period allows chain to catch up the phase angle lagging previously. Consequently, the overall trajectory of the chain follows the field without significant time delay in the strongest field of $H_p = 124.48$ Oe. As to the weaker perpendicular field strengths, such as $H_p = 29.02$ Oe, and 70.88 Oe also shown in Fig. 7a, the trajectory patterns of the external fields are closer to the sinusoidal wave compared to the previous case of $H_p = 124.48$ Oe. Variations in instantaneous angular speeds are less significant with shorter stagnant periods for allowing the chains to catch up the field in time. This explains the trajectory patterns appearing less synchronous with apparent time delays for these cases of smaller perpendicular field strengths.

The distinct behaviors regarding the trajectories of the chains in different perpendicular field conditions can also be distinguished from Fig. 7b. The nearly synchronous oscillation between the chain and field in the case of $H_p = 124.48$ Oe results in no significant phase lags, except near $t = 0$, $P/2$, P and $3P/2$, when the instantaneous phase lags are enormous. On the other hand, apparent phase lags appear throughout the entire period in the cases of the weaker fields of $H_p = 29.02$ and 70.88 Oe. Nevertheless, their maximum instantaneous lags are smaller than those shown in the strongest field of $H_p = 124.48$ Oe.

The actual amplitudes of the particle chains subjected to various perpendicular field strengths are also shown in Fig. 5. According to the nature of the field configuration, the amplitude of external fields, expressed as $\theta_{\text{Amax}} = \tan^{-1}(H_p/H_d)$, would approach 90° asymptotically by raising the strength of its perpendicular component. Similar asymptotical trends are also observed for chains consisting of the same number of particles subjected to increasing perpendicular field strengths. Note, for P19 and P21 chains, stable chaining structures can only be sustained up to a perpendicular field strength of $H_p = 42.03$ Oe. Fractures occur when the field strength exceeds $H_p = 56.7$ Oe. The sustainable field strength for a P15 chain is higher at $H_p = 70.88$ Oe, while P9 chain remains stable throughout the range of field strength experimented up to $H_p = 163.3$ Oe. Further discussion regarding the rupturing failures of microchains will be presented in a later section.

3.1.3 *Effects of directional field strength*

The effects of the directional field are demonstrated by experimenting on a P15 chain under different $H_d = 16.37$ and 24.15 Oe strengths in a fixed perpendicular field of $H_p = 29.02$ Oe and $f = 1$ Hz. The major role of the directional field is to provide magnetic inter-particle attractions to form a chain. On the other hand, the presence of a directional field always tends to dampen the overall oscillating pattern, i.e., reducing amplitude. Figure 8a confirms a lower amplitude is associated with the external field of a stronger directional component. However, it is interesting to note the actual amplitudes of the two presented cases remain nearly the same, while a longer time delay occurs in a weaker directional field. The similar amplitudes are the result of the counter effects of directional field strength to the magnetic torque shown in Eq. (1). Because of lower dampening effects, the chain in a weaker directional field experiences higher phase lags ($\Delta\theta_L$), as shown in Fig. 8b. Meanwhile, the overall magnitude of the dipole moment ($\vec{m}$), which can be expressed as $\vec{m} = \frac{4}{3}\pi a^3 \mu_0 \chi \vec{H}$ for a single particle, is decreased in a weaker directional field. These counter effects, for example, increasing phase lags and decreasing dipole moment, offset the influences to the magnetic torque and explain the similar amplitudes shown in Fig. 8a. The insignificant effects on the magnetic torque lead to similar trajectories of these cases till $t = P/3$, when the chain in $H_d = 24.15$ Oe crosses over its corresponding field trajectory. After this time, the chain in such a stronger directional field moves in reverse due to the sign change of the phase lags, which can be observed in Fig. 8b. However, the reverse motion of the chain subjected to a weaker directional field of $H_d = 16.37$ Oe does not occur until a later time at $t = 2P/5$,

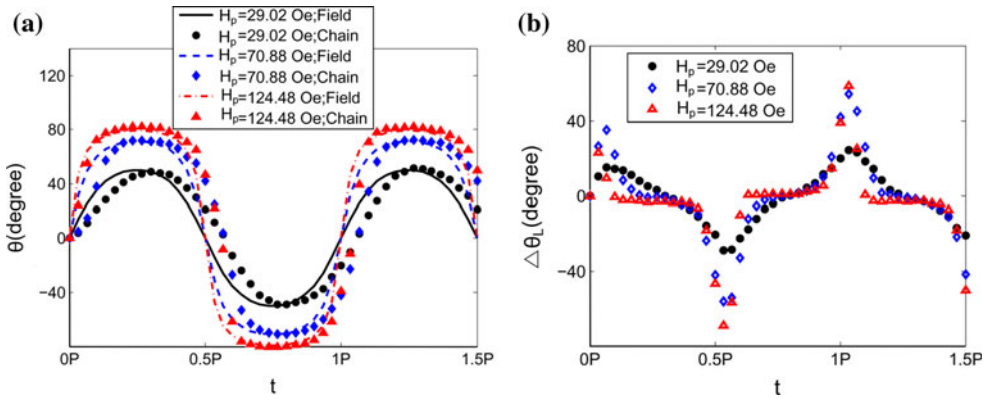

Fig. 7 **a** Trajectories of phase angles (θ) of external fields and P9 chain in various perpendicular field strengths. The chain oscillates more synchronously with the external field in stronger field strengths. **b** Evolutions of phase angle lag ($\Delta\theta_L$) for the P9 chain in various perpendicular field strengths. Nearly vanishing phase lags for the case of $H_p = 124.48$ Oe, except in the vicinity of the peaks, indicates almost synchronous oscillation between the chain and field

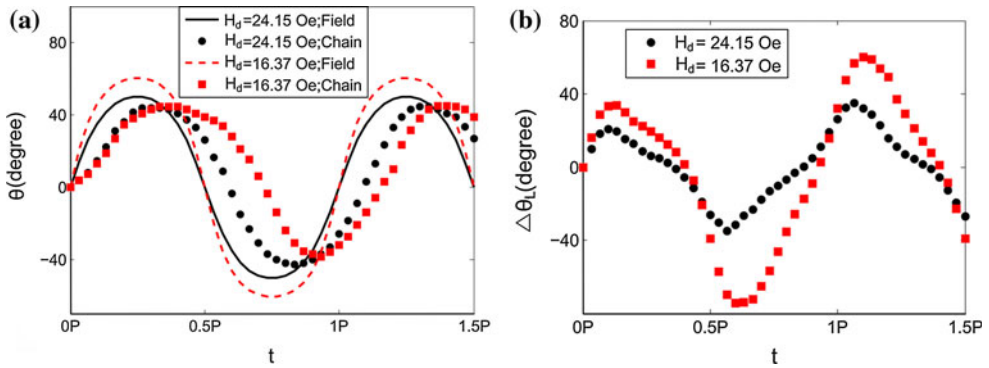

Fig. 8 **a** Trajectories of phase angle (θ) of external fields and P15 chain subjected to a field condition of $H_p = 29.02$ Oe and $f = 1$ Hz in various directional field strengths (H_d). Nearly the same amplitudes of oscillating chains are observed. The trajectory of the chain subjected to the weak field shows longer time delay. **b** Evolutions of phase angle lag ($\Delta\theta_L$) for the P15 chain in various directional field strengths. The chain in the weaker directional field leads to higher phase lags

when $\Delta\theta_L$ vanishes. This later time of reversed motion in a weaker field results in a longer time shift of its phase trajectory to its corresponding field, as shown in Fig. 8b.

3.2 A rupture chain

It has been previously mentioned that, rupturing failures occur when the external field strength or chain's length exceed certain critical values. Understandings of such fractures are also crucial in applications, and worthy of special attention. Figure 9 shows snapshot images near the times of rupture for three representative cases, for example, P15, P16 and P20 chains in fields of $H_p = 56.72$, 65.25, and 87.36 Oe, respectively, with a fixed $H_d = 17.01$ Oe. A general pattern of ductile chain fracture is observed, so the chains experience nearly symmetric S shape deformation shortly before $t = P/2$ and breakup from the sides at near $t = P/2$. It has been agreed the dynamics of a magnetic chain under a rotational field are governed by the dimensionless parameter Mason number (Mn), which compares the magnitudes of viscous drag and radial magnetic attraction. The Mason number is defined as (Melle et al. 2003; Biswal and Gast 2004b; Roy et al. 2009)

$$Mn = \frac{32\eta\omega}{\mu_0\chi^2\left|\vec{H}\right|^2}. \tag{3}$$

A larger Mason number indicates a stronger hydrodynamic drag or weaker inter-particle magnetic attraction. Note, the Mason numbers in the present oscillating field are transient measurements because of the variation in angular speed, instead of constant in the conventional rotational case. In addition, the theoretical model suggests the critical length (or number of particle N_c) of a stable chain in a rotational field is inversely proportional to the square root of the Mason number (Melle and Martin 2003), i.e., $N_c \sim 1/Mn^{1/2}$. We follow the same argument in the present

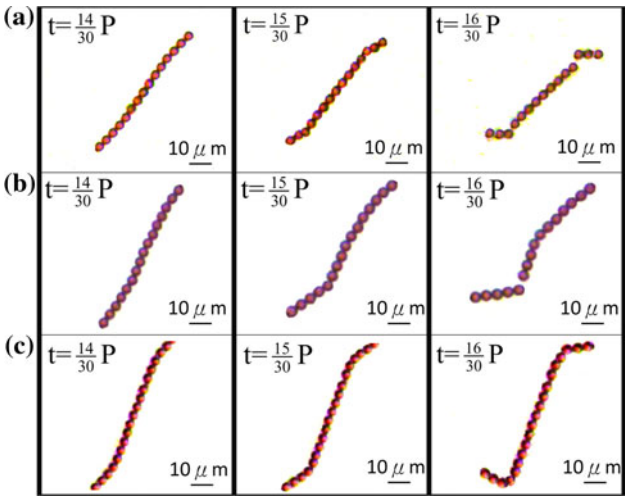

Fig. 9 Snapshot images of **a** P15 chain in $H_p = 56.72$Oe, **b** P16 chain in $H_p = 56.72$ Oe and **c** P20 chain in $H_p = 87.36$ Oe. A weaker directional field of $H_d = 17.01$ Oe is applied. The chain is bent and ruptured from both sides near $t = P/2$

oscillating field, and the corresponding values of $(N^*Mn^{1/2})$ of these three representative cases before their ruptures are displayed in Fig. 10.

Some interesting features can be identified regarding the values of $(N^*Mn^{1/2})$ at different times. First, all three curves follow a close trajectory, suggesting the universality of such a dimensionless parameter in the present situation of oscillating chains. In addition, the local maxima of $(N^*Mn^{1/2})$ always occur right after $t = 0$ and before $t = P/2$, when the phase angles of the external field vanish. This feature can be understood by the definition of the Mason number and corresponding phase trajectories of the chains.

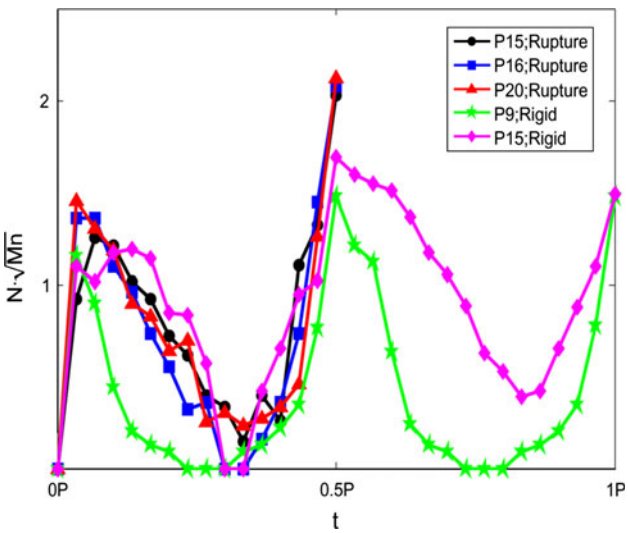

Fig. 10 Values of $N^*Mn^{1/2}$ for cases demonstrated in Fig. 9 and reference cases of the P9 and P15 chains. All three curves of the rupturing chains follow a close trajectory with local maxima near $t = 0P$, $P/2$. Ruptures occur at $t = P/2$ when $N^*Mn^{1/2} > 2$

To better illustrate the evolution of $(N^*Mn^{1/2})$, the particular cases of P9 and P15 chains in different field strengths, which both show rigid oscillation without any structure failures, are also included in Fig. 10. The phase trajectories for these particular P9 chain and P15 chains are referred to in Figs. 3a and 8a, respectively. According to the expression in Eq. (3), the magnitude of the Mason number is directly proportional to the chain's local angular speed, but inverse to the square of the local field strength. The present field configuration leads to the smallest overall field strengths at $t = 0$, $P/2$, and P, when the perpendicular field vanishes, i.e., $H_p = 0$. In addition, maximum angular speeds can also be observed at these times from both the phase trajectories. As a result, for a chain of synchronously periodical oscillation with the external field, such as the P9 chain, the local maxima of the Mason number would always appear at these times. This argument closely agrees with the actual measurements shown in Fig. 10. Nevertheless, the value of the Mason number at $t = 0$ appears smaller than at $t = P/2$ and P, which is mainly due to a lower angular speed of the sudden start.

The final and also the most interesting observation is all the ruptures occur when $N^*Mn^{1/2} > 2$. The results confirm that the theoretical argument of $N_c \sim 1/Mn^{1/2}$ obtained in a rotational field is also suitable in the present oscillating field condition. Based on the results, a critical value of $1.7 < N^*Mn^{1/2} < 2.0$ is suggested to the present experimental configuration. Note, the above observations are generally valid for many other experiments.

According to the above discussion, there are crucial timings, such as $t = 0$, $P/2$ and P, when the instantaneous values of the Mason number are maximum and could lead to a rupture of the chain. Because of the influences of the initial start, the Mason numbers at $t = 0$ of the representative cases shown in Figs. 9 and 10 are lower than the critical value to avoid temporary fracture until the next barrier near $t = P/2$. A question arises if there are situations where ruptures occur near the first barrier at $t = 0$. To validate such an argument, experiments which would lead to a higher initial Mason number are designed. To achieve such a condition, it is worth evaluating the influences of the field components on the values of the Mason number. If a chain oscillates in perfect synchrony with the external field, the theoretical values of the Mason number in different field configurations, denoted as Mn_F, are plotted in Fig. 11. Note, these values can be used as the upper limits of the chains, since the actual angular speeds of the oscillating chains are always smaller than the field due to viscous drags. Figure 11 clearly shows the values of the Mason number are much more sensitive to the directional component. This fact is not surprising, since the Mason number is defined as the radial attraction between particles, which is more relevant to the directional field applied as the main chaining mechanism.

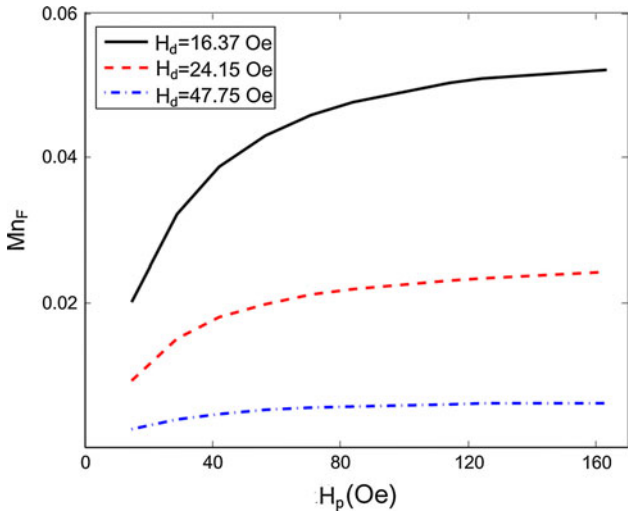

Fig. 11 Maximum values of Mason number (Mn_F), obtained when chain oscillates perfectly synchronically with the external field, in various field configurations. The Mason number is much more sensitive to the directional component

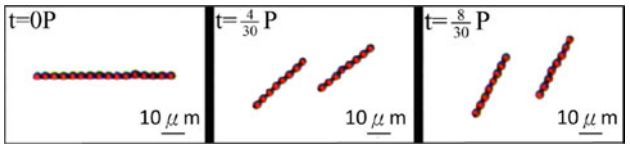

Fig. 12 Sequential images of the P16 chain in a weak directional field. Brittle chain fracture occurs at the center immediately after motion

A representative case of a P16 chain in an even weaker directional field is shown in Fig. 12, so the initial values of the Mason number as well as ($N^*Mn^{1/2}$) are increased effectively. As expected, fracture occurs immediately after the motion. Somewhat surprisingly, the pattern of fracture differs from the previous cases shown in Fig. 9. Instead of ruptures on the sides as shown in Fig. 9, the chain breaks at its center. In addition, the rupture can be categorized as a brittle chain fracture, since no apparent deformation appears.

Understanding the distinct patterns of ruptures relies on detailed investigations of force distributions at individual particles, which is beyond the scope of the present study. Nevertheless, the results have further justified the appropriateness of applying the Mason number and the number of particles as important factors to the determination of the chain's rupture.

4 Conclusion

In the present work, the motion of a magnetic-particle chain subjected to an oscillating field is thoroughly experimented and analyzed. This particular device possesses potential applications in the MEMS systems, including micromixers, actuators, and swimmers. The dynamics of an oscillating chain are determined by the driving magnetic torque and the induced hydrodynamic resistance. We demonstrate the chain's motion can be successfully manipulated by the control parameters, such as the number of particles in the chain and the strength of the external field. Distinct behaviors, such as rigid body oscillations and bending distortions to rupture failures, are recorded in various conditions of the control parameters.

Deviation of the actual phase angle trajectory of an oscillating chain from the external field is a major issue of interest in applications because it provides useful information regarding effective manipulation of the microchain. Major measurements, such as synchronization and amplitude, are discussed in detail to elucidate the deviations. It is concluded the oscillation of a shorter chain, whose induced drag is smaller, more closely follows the external field in the form of a rigid body oscillation. On the other hand, external field strength does not affect the chain's trajectory in a straightforward manner. Even if the chain in a stronger field generally oscillates more synchronically with the field, the influences of the directional and perpendicular field components on the local measurements of interest, such as time shift of the trajectory, amplitudes of oscillation, and instantaneous phase angle lags, show slight differences. By increasing the strength of the directional field, all local measurements of interest tend to approach the external field consistently, i.e., a shorter time delay, a smaller amplitude difference and less significant phase lags, throughout the entire period. Nevertheless, a stronger perpendicular field causes more significant instantaneous phase lags at $t = P/2$, P and $3P/2$ etc.

Rupturing failures were also demonstrated if the external field strength or number of particles contained in the chain exceeded a critical value. The patterns of ruptures could be either ductile fracture, that is, a chain is bent to a S shape followed by rupture from its sides at near $t = P/2$, or brittle fracture, which occurs at the center immediately after motion. In general, a brittle fracture is preferable in a field configuration associated with a weaker directional component. The experimental results confirm the criterion to maintain a stable chain can be determined by the value of $N^*Mn^{1/2}$, which is obtained theoretically in a rotational field. The value of such a criterion to sustain a stable chain is suggested to be within the range of $1.7 < N^*Mn^{1/2} < 2.0$ in the present experimental configuration.

A final remark regarding the potential scalability of the present process to smaller particles and higher field frequencies is worthy to be addressed. The experiments of various particle sizes in higher field frequencies had been demonstrated successfully in microswimmers (Dreyfus

et al. 2005; Li et al. 2012), even detailed dynamics of chains would be strongly affected both by the particle size and the field frequency. As demonstrated in Eqs. (1) and (2), the induced viscous dissipation and the magnetic driving force depend explicitly on the particle size and the angular speed, respectively. Nevertheless, the overall mechanism should be consistent and similar to the present study. In addition, the recent development of microfluidic devices in superconducting magnets (Vojtisek et al. 2012) could be potentially applied to provide sufficient field strength to the present configuration. These progresses support the applicability of such a configuration in practical MEMS systems.

Acknowledgments The financial support from the National Science Council of Republic of China (Taiwan) through Grant NSC 99-2221-E-009-057-MY3 is acknowledged.

References

Biswal S, Gast A (2004a) Micromixing with linked chains of paramagnetic particles. Anal Chem 76:6448–6455

Biswal S, Gast A (2004b) Rotational dynamics of semiflexible paramagnetic particle chains. Phys Rev E 69:041406

Dreyfus R, Baudry J, Roper ML, Fermigier M, Stone HA, Bibette J (2005) Microscopic artificial swimmers. Nature 437:862

Gijs M (2004) Magnetic bead handling on-chip: new opportunities for analytical application. Microfluid Nanofluid 1:22–40

Kang TG, Hulsen M, Anderson P, den Toonder J, Meijer H (2007) Chaotic mixing induced by a magnetic chain in a rotating magnetic field. Phys Rev E 76:066303

Karle M, Wohrle J, Miwa J, Paust N, Roth G, Zengerle R, von Stetten F (2011) Controlled counter-flow motion of magnetic bead chains rolling along microchannels. Microfluid Nanofluid 10:935–939

Lacharme F, Vandevyver C, Gijs MAM (2009) Magnetic beads retention device for sandwich immunoassay comparison of off-chip and on-chip antibody incubation. Microfluid Nanofluid 7:479–487

Li YH, Sheu ST, Pai JM, Chen CY (2012) Manipulations of vibrating micro magnetic particle chains. J Appl Phys 111:07A924

Martin J, Shea-Roher L, Solis K (2009) Strong intrinsic mixing in vortex magnetic fields. Phys Rev E 80:016312

Melle S, Martin J (2003) Chain model of a magnetorheological suspension in a rotating field. J Chem Phys 118(21):9875

Melle S, Fuller G, Rubio M (2000) Structure and dynamics of magnetorheological fluids in rotating magnetic fields. Phys Rev E 61(4):4111–4117

Melle S, Calderon O, Fuller G, Rubio M (2002a) Polarizable particle aggregation under rotating magnetic fields using scattering dichroism. J Colloid Interface Sci 247:200

Melle S, Calderon O, Rubio M, Fuller G (2002b) Rotational dynamics in dipolar colloidal suspensions: video microscopy experiments and simulations results. J Non Newton Fluid Mech 102(2): 135–148

Melle S, Calderon O, Rubio M, Fuller G (2003) Microstructure evolution in magnetorheological suspensions governed by Mason number. Phys Rev E 68:041503

Petousis I, Homburg E, Derks R, Dietzel A (2007) Transient behaviour of magnetic micro-bead chains rotating in a fluid by external fields. Lab Chip 7:1746

Roy T, Sinha A, Chakraborty S, Ganguly R, Puri I (2009) Magnetic microsphere-based mixers for microsroplets. Phys Fluids 21:027101

Terray A, Oakey J, Marr D (2002) Microfluidic control using colloidal devices. Science 296:1841–1844

Vojtisek M, Tarn M, Hirota N, Pamme N (2012) Microfluidic devices in superconducting magnets-on-chip free-flow diamagnetophoresis of polymer particles and bubbles. Microfluid Nanofluid. doi:10.1007/s10404-012-0979-6

Vuppu A, Garcia A, Hayes M (2003) Video Microscopy of dynamically aggregated paramagnetic particle chains in an applied rotating magnetic field. Langmuir 19:8646

Weddemann A, Wittbracht F, Auge A, Hutten A (2011) Particle flow control by induced dipolar interaction of superparamagnetic microbeads. Microfluid Nanofluid 10:459–463

Wittbracht F, Weddemann A, Eickenberg B, Hutten A (2012) On the direct employment of dipolar particle interaction in microfluidic system. Microfluid Nanofluid (submitted)